

# Resonant X-Ray Scattering from URu<sub>2</sub>Si<sub>2</sub>

Tatsuya Nagao\* and Jun-ichi Igarashi<sup>1</sup>

*Faculty of Engineering, Gunma University, Kiryu, Gunma 376-8515*

<sup>1</sup>*Faculty of Science, Ibaraki University, Mito, Ibaraki 310-8512*

(Received October 26, 2018)

Based on a localized crystal electric field model for the U<sup>4+</sup> in the (5*f*)<sup>2</sup>-configuration, we analyze the resonant x-ray scattering spectra around U *M*<sub>IV</sub> and *M*<sub>V</sub> edges in URu<sub>2</sub>Si<sub>2</sub>, taking full Coulomb and spin-orbit interactions into account. We consider two level schemes, a singlet model of Santini and Amoretti and a doublet model of Ohkawa and Shimizu, and assume the antiferroquadrupolar order and the antiferromagnetic order as candidates for the ambient pressure phase and the high pressure phase. It is found that the spectral shapes as a function of photon energy are independent of the assumed level scheme, but are quite different between the antiferroquadrupole and antiferromagnetic phases. This may be useful to determine the character of the ordered phase.

KEYWORDS: resonant x-ray scattering, URu<sub>2</sub>Si<sub>2</sub>, singlet scheme, doublet scheme

## 1. Introduction

The ternary intermetallic compound URu<sub>2</sub>Si<sub>2</sub> has been attracting much attentions since the discovery of the coexistence of antiferromagnetic (AFM) ordering below  $T_0 = 17.5$  K and superconductivity below  $T_C = 1.2$  K.<sup>1</sup> The ordering pattern of the AFM order is type-I structure with the propagation vector  $\mathbf{Q} = (001)$  along the *c*-axis (Fig. 1). The phase transition at  $T_0$  is characterized by bulk anomalies such as specific heat,<sup>2</sup> linear susceptibility,<sup>2</sup> non-linear susceptibility,<sup>3,4</sup> thermal expansion<sup>5</sup> and electrical resistivity,<sup>6</sup> strongly indicating that the transition is of second order.

The observed magnetic moment is unusually tiny ( $\mu_{\text{ord}} \sim (0.03 \pm 0.01)\mu_B$  per U ion at saturation).<sup>7-9</sup> It is too small to account for the observed bulk anomalies. The magnetic excitation spectra shows energy gap below  $T_0$  according to neutron scattering experiments.<sup>10</sup> Under the magnetic field, the magnetic moment and the magnetic excitation gap exhibit the different field dependencies.<sup>11</sup> Based upon these observations, it is widely believed that, the AFM order below  $T_0$  is merely a secondary order and there exists some unknown primary order, so-called "hidden order (HO)".<sup>12</sup> As for the true nature of the HO phase, various competing theoretical possibilities have been demonstrated. For instance, the antiferroquadrupole (AFQ) order,<sup>13-17</sup> the multispin correlation,<sup>18</sup> the unconventional spin density wave,<sup>19</sup> inhomogeneous orbital current,<sup>20-22</sup> Jahn-Teller distortions<sup>23</sup> and so on were proposed. However, it is safe to say that the microscopic mechanism governing the whole phenomena is still in a matter of controversy.

Recently, neutron scattering and <sup>29</sup>Si NMR experiments were performed under pressure.<sup>24-29</sup> The measurements are interpreted that not the magnitude of the AFM moment but the volume fraction of the AFM phase is tiny below  $T_0$ . The volume fraction of the AFM phase is estimated about 1 % at ambient pressure while the magnitude of the moment is  $0.25 \mu_B$  per U ion. Another discovery of importance is the presence of the phase tran-

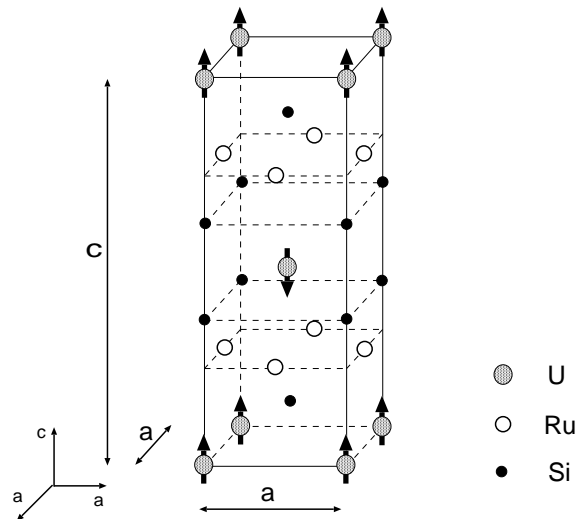


Fig. 1. Crystal structure of body-centered tetragonal URu<sub>2</sub>Si<sub>2</sub>. The arrows show the magnetic structure corresponding to a wave vector  $\mathbf{Q} = (001)$ .

sition around  $p_C = 1.5$  GPa, accompanied by the discontinuous changes of the quantities such as  $T_0$ , the lattice constant and the value of the magnetic moment. In high pressure phase, the AFM order extends uniformly throughout the entire sample. It exhibits a three dimensional AFM Ising behaviors with the saturated staggered moment  $\sim 0.4\mu_B/\text{U}$  and with the same magnetic structure as in the ambient pressure (HO) phase.<sup>24</sup>

One of the promising efforts to elucidate the nature of the order parameter in the *d* and *f* electron systems is the resonant x-ray scattering (RXS) measurement. By utilizing the facts that the method is element specific and level specific, and that the RXS intensity generally shows special incident photon polarization and azimuthal angle dependencies, we can deduce valuable information to understand the physical properties of subjects. In *4f* systems, for example, the RXS peaks at the Ce *L*<sub>III</sub> absorption edge in CeB<sub>6</sub> are interpreted as the direct obser-

\*E-mail address: tnagao@phvs.sci.gunma-u.ac.jp

variation of the AFQ ordering<sup>30–33</sup> while the peaks at the Dy  $L_{III}$  edge in DyB<sub>2</sub>C<sub>2</sub> are explained as the consequence of lattice distortion.<sup>34–37</sup>

For actinide compounds, the  $M_{IV,V}$  edge resonance is available for superlattice Bragg spots. Since the dipole process gives rise to a transition from the  $3d$  states to the  $5f$  states which drive ordering, the RXS signal is more direct than those at the  $K$ -edge in the transition-metal compounds. In transition metal oxides, the RXS signals at the  $K$ -edge involve the transition from the  $1s$  state to the  $4p$  states. Since the  $4p$  states are considerably extending in space, they are very sensitive to electronic structures at neighboring sites. Thereby the RXS signal on the orbital ordering superlattice spots are mainly controlled by lattice distortion.<sup>38–40</sup>

Isaacs *et al.* reported the resonant enhancements corresponding to the U  $M_{IV}$  edge upon URu<sub>2</sub>Si<sub>2</sub> at ambient pressure below  $T_0$ .<sup>41</sup> The measured RXS peak intensity at the prohibited Bragg spot (003) develops linearly over an unusually wide range of temperature from  $T_0$  down to about 3 K, then ceases to grow when superconductivity sets in. The width of the spectra is evaluated about 5 eV. Later, Lidström *et al.* have observed the peak intensities at U  $M_{IV}$  and  $M_V$  edges from U<sub>1-x</sub>Np<sub>x</sub>Ru<sub>2</sub>Si<sub>2</sub> alloys with  $x = 0.1, 0.5$  and  $1.0$  also using the RXMS technique.<sup>42</sup>

In this paper, we analyze the RXS spectra in the low temperature phases of URu<sub>2</sub>Si<sub>2</sub> on the basis of a localized model under the crystal electric field (CEF). Although the CEF-like excitations are not clear in the high temperature phase, a localized picture can explain well the behavior of various quantities such as the specific heat and the magnetic susceptibility.<sup>13,24,25</sup> Since the CEF parameters are not known, the level schemes are not definitely determined. There are two prevailing schemes, the “singlet” scheme of Santini and Amoretti<sup>13</sup> and the “doublet” scheme of Ohkawa and Shimizu.<sup>17</sup> On the basis of the two level schemes, we consider both the AFQ and AFM phases, and calculate the RXS spectra as a function of photon energy and of azimuthal angle. We find that the calculated spectral shapes are independent of the assumed scheme, although the intensities are quite different.<sup>43</sup> Thereby the RXS spectral shapes depend only on the assumed order parameter. The RXS spectral shapes as a function of energy are found quite different between the AFQ phase and the AFM phase. In principle, this may make it possible to distinguish whether the experimental signals come from the HO phase or from the AFM domains. Unfortunately available experimental spectra are not clear enough to distinguish those differences.<sup>41,42</sup> Shishidou *et al.*<sup>44</sup> calculated the RXS spectra in the AFQ phase within the doublet scheme. The present calculation agrees with their result.

The present paper is organized as follows. In §2, we briefly summarize the theoretical framework of RXS. In §3, we discuss two level schemes under the CEF on the basis of the localized  $5f$  model, and the AFQ and AFM states as candidates of the ground state under these schemes. The intermediate states are briefly discussed. In §4, numerical results of the RXS spectra are presented in comparison with the experiments. A summary and dis-

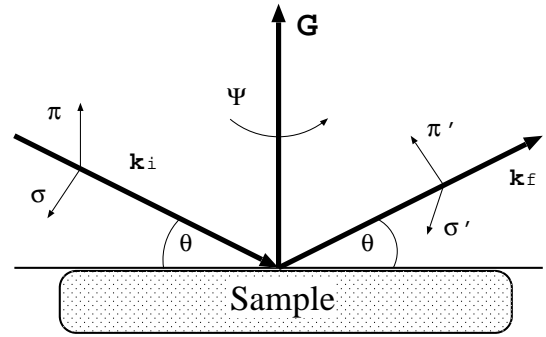


Fig. 2. Geometry of the RXS experiment. Photon with polarization  $\sigma$  or  $\pi$  is scattered into the state of polarization  $\sigma'$  or  $\pi'$  at Bragg angle  $\theta$ .

cussion are given in §5. In Appendix, general expressions of the matrix elements of the scattering amplitude are given. It is proved that the RXS spectral shapes are independent of the assumed level schemes.

## 2. Theoretical Framework of RXS

We consider the experimental situation of RXS shown in Fig. 2. The incident photon with frequency  $\omega$  and wave vector  $\mathbf{k}_i$  is scattered into the state with frequency  $\omega$  and wave vector  $\mathbf{k}_f$ . The sample is rotated around the scattering vector  $\mathbf{G} (= \mathbf{k}_f - \mathbf{k}_i)$  by azimuthal angle  $\psi$ . The resonant enhancement is found at the U  $M_{IV}$  and  $M_V$  absorption edges, where the  $3d$  core electron is virtually excited to the  $5f$  states then falls to the core level in the dipolar ( $E_1$ ) process. The tuning energy for  $M_{IV}$  edge is around 3.728 keV and that for  $M_V$  is around 3.550 keV. The scattering tensor can be well approximated by a sum of the contributions from each site of the created core hole. Therefore the RXS intensity in the  $E_1$  process is given by

$$I_{\mu \rightarrow \mu'}(\mathbf{G}, \omega) \propto \left| \sum_{\alpha\alpha'} P_{\alpha}^{\mu'} M_{\alpha\alpha'}(\mathbf{G}, \omega) P_{\alpha'}^{\mu} \right|^2, \quad (2.1)$$

with

$$M_{\alpha\alpha'}(\mathbf{G}, \omega) = \frac{1}{\sqrt{N}} \sum_j \sum_{\Lambda} e^{-i\mathbf{G} \cdot \mathbf{r}_j} \times \frac{\langle \psi_0 | x_{\alpha}(j) | \Lambda \rangle \langle \Lambda | x_{\alpha'}(j) | \psi_0 \rangle}{\hbar\omega - (E_{\Lambda} - E_0) + i\Gamma}, \quad (2.2)$$

where  $N$  is the number of U ions. The  $|\psi_0\rangle$  represents the ground state with energy  $E_0$ , and  $|\Lambda\rangle$  represents the intermediate state with energy  $E_{\Lambda}$ . The dipole operators  $x_{\alpha}(j)$ 's are defined as  $x_1(j) = x$ ,  $x_2(j) = y$ , and  $x_3(j) = z$  in the coordinate frame fixed to the crystal axes with the origin located at the center of site  $j$ . The  $P^{\mu}$  and  $P^{\mu'}$  denote the geometrical factors for the incident photon and the scattered photon, whose explicit expressions are given in ref. 37. The  $\Gamma$  describes the life-time broadening width of the core hole.

Table I. Slater integrals and spin-orbit interaction parameters within the HFA (in units of eV).<sup>45</sup>

the (3d) <sup>10</sup> (5f) <sup>2</sup> configuration					
$F^k(3d, 3d)$	$F^k(3d, 5f)$	$F^k(5f, 5f)$	$G^k(3d, 5f)$		
$F^0$ 177.7		$F^0$ 18.84			
$F^2$ 90.80		$F^2$ 9.519			
$F^4$ 58.48		$F^4$ 6.228			
		$F^6$ 4.573			
$\zeta_{3d} = 74.611$		$\zeta_{5f} = 0.277$			
the (3d) <sup>9</sup> (5f) <sup>3</sup> configuration					
$F^0$ 178.7	$F^0$ 28.08	$F^0$ 19.82	$G^1$	2.011	
$F^2$ 91.39	$F^2$ 2.570	$F^2$ 10.03	$G^3$	1.216	
$F^4$ 58.87	$F^4$ 1.194	$F^4$ 6.574	$G^5$	0.850	
		$F^6$ 4.832			
$\zeta_{3d} = 75.619$		$\zeta_{5f} = 0.318$			

### 3. Electronic Structure

#### 3.1 The ground state

We adopt a localized description that each U ion is in the (5f)<sup>2</sup>-configuration. The Hamiltonian of U ions consists of the intra-atomic Coulomb interaction between 5f electrons and the spin-orbit interaction (SOI) of 5f electrons, which are represented by 91 states in the (5f)<sup>2</sup>-configuration. We evaluate the Slater integrals for the Coulomb interaction in the 5f states and the SOI parameters within the Hartree-Fock approximation (HFA).<sup>45</sup> The values are listed in Table I. It is known that the values for the isotropic part of the Slater integral  $F^0$  are considerably reduced due to large screening effects. We reduce the value by multiplying a factor 0.25. On the other hand, the values for the anisotropic part of the Slater integrals are not screened so much. We slightly reduce them by multiplying a factor 0.8. We diagonalize the Hamiltonian, and obtain nine degenerate states belonging to the  $J = 4$  subspace as the lowest-energy state. Note that these states of  $J = 4$  are slightly deviated from those of the LS coupling scheme with  $L = 5$  and  $S = 1$  due to the SOI.

It is known that the crystal structure of URu<sub>2</sub>Si<sub>2</sub> is the body-centered tetragonal (bct) ThCr<sub>2</sub>Si<sub>2</sub> structure (I4/mmm) with lattice constants  $a = 4.124\text{\AA}$  and  $c = 9.582\text{\AA}$  at  $T = 4.2\text{ K}$  (Fig. 1).<sup>46</sup> Under the bct symmetry, the degeneracy in the  $J = 4$  subspace is lifted by the CEF Hamiltonian, which may be expressed as

$$H_{\text{cry}} = \sum_k \sum_q B_k^q O_k^q, \quad (3.3)$$

where  $O_k^q$ 's denote the Stevens operator equivalence. The CEF parameters  $B_k^q$ 's take non-zero values for  $(k, q) = (2, 0), (4, 0), (4, 4), (6, 0)$  and  $(6, 4)$ . The eigenstates of the Hamiltonian split into five singlets and two doublets as listed in Table II, where the  $\epsilon, \gamma, \alpha$  depend on the CEF parameters. At present, it is difficult to determine the CEF parameters in a convincing way. In the following, we discuss two prevailing CEF level schemes.

#### 3.1.1 Singlet scheme

Analyzing the temperature dependences of magnetic susceptibility and specific heat, Santini and Amoretti<sup>13</sup> have proposed a CEF level scheme that the lowest three

Table II. Eigenstates of the CEF Hamiltonian eq. (3.3) with  $|M\rangle$  denotes the state of  $J_z = M$ .

$\Gamma_{t1}^{(1)}$	$\epsilon( +4\rangle +  -4\rangle) + \gamma 0\rangle$
$\Gamma_{t1}^{(2)}$	$\frac{\gamma}{\sqrt{2}}( +4\rangle +  -4\rangle) - \sqrt{2}\epsilon 0\rangle$
$\Gamma_{t2}$	$\frac{1}{\sqrt{2}}( +4\rangle -  -4\rangle)$
$\Gamma_{t3}$	$\frac{1}{\sqrt{2}}( +2\rangle +  -2\rangle)$
$\Gamma_{t4}$	$\frac{1}{\sqrt{2}}( +2\rangle -  -2\rangle)$
$\Gamma_{t5}^{(1)}$	$\cos\alpha  \pm 3\rangle + \sin\alpha  \mp 1\rangle$
$\Gamma_{t5}^{(2)}$	$\sin\alpha  \pm 3\rangle - \cos\alpha  \mp 1\rangle$

states become  $\Gamma_{t3}$  (or  $\Gamma_{t4}$ ),  $\Gamma_{t1}^{(1)}$  and  $\Gamma_{t2}$  in order, with energy separation 3.8 meV, 9.6 meV from the lowest state, respectively, and that the other states have energies more than  $\sim 40$  meV higher than the above. This scheme has been considered for bringing about the AFQ ordering at low temperatures. It successfully reproduced the experimental magnetic susceptibility and specific heat in a wide temperature region.<sup>13</sup>

Within the states  $\Gamma_{t3}$ ,  $\Gamma_{t1}^{(1)}$  and  $\Gamma_{t2}$ , the dipole operator  $J_z$  and the quadrupole operators  $O_{x^2-y^2} \equiv \frac{\sqrt{3}}{2}(J_x^2 - J_y^2)$ ,  $O_{xy} \equiv \frac{\sqrt{3}}{2}(J_x J_y + J_y J_x)$  are represented as

$$J_z = \frac{8\epsilon}{\sqrt{2}} \begin{pmatrix} 0 & 0 & 0 \\ 0 & 0 & 1 \\ 0 & 1 & 0 \end{pmatrix}, \quad (3.4)$$

$$O_{x^2-y^2} = \sqrt{6}(\sqrt{7}\epsilon + 3\sqrt{5}\gamma) \begin{pmatrix} 0 & 1 & 0 \\ 1 & 0 & 0 \\ 0 & 0 & 0 \end{pmatrix}, \quad (3.5)$$

$$O_{xy} = \sqrt{7} \begin{pmatrix} 0 & 0 & i \\ 0 & 0 & 0 \\ -i & 0 & 0 \end{pmatrix}. \quad (3.6)$$

Another choice of the states  $\Gamma_{t4}$ ,  $\Gamma_{t1}^{(1)}$ ,  $\Gamma_{t2}$  makes the matrix of  $O_{x^2-y^2}$  and that of  $O_{xy}$  interchanged. The  $\epsilon$  and  $\gamma$  are estimated as  $-0.6775$  and  $0.2864$ , according to Santini and Amoretti's analysis.<sup>13</sup> For describing the AFQ phase, we add a term  $\lambda Q \langle Q \rangle$  on the basis of the mean-field approximation to the multipolar interaction. Here  $\langle Q \rangle$  is the staggered moment of one of the quadrupole  $O_{x^2-y^2}$  or  $O_{xy}$  and  $\lambda = 0.185$  meV is a mean-field coefficient.<sup>13,47</sup> The self-consistent solution gives us the AFQ ordering at low temperatures;  $|\langle Q \rangle| = 12.1$  at zero temperature. The above expressions indicate that the  $O_{x^2-y^2}$  (or  $O_{xy}$ ) ordering is most realized at low temperatures through the off-diagonal element between the lowest and the first excited states.

For describing the AFM phase, we now introduce a molecular field term  $\lambda' J_z \langle J_z \rangle$ , where  $\langle J_z \rangle$  is the staggered dipole moment. Since  $J_z$  has no matrix element to the lowest energy level (see eq. (3.4)), the molecular field energy has to exceed the crystal field energy for giving rise to the AFM phase at low temperature. For  $\lambda' > 0.468$  meV, a self-consistent solution exists as  $|\langle J_z \rangle| > 3.490$  with  $\mu/\mu_B = |\langle L_z + 2S_z \rangle| = 2.887$ . For instance, when  $\lambda' = 0.5$  meV,  $|\langle J_z \rangle| = 3.540$ , and the staggered moment becomes  $\mu = 2.925\mu_B$ . Therefore the AFM ordering can be brought about only with assuming a large intersite U-

U coupling. This staggered moment is much larger than the experimental value  $\mu \simeq 0.4\mu_B$  in the pressure range between  $p = 1.5$  and  $2.8$  GPa.<sup>24,25</sup>

### 3.1.2 Doublet scheme

Ohkawa and Shimizu<sup>17</sup> have proposed another model that the lowest energy levels belong to the doublet  $\Gamma_{t_5}^{(1)}$  or  $\Gamma_{t_5}^{(2)}$ . This doublet scheme naturally gives rise to the AFQ and AFM orderings under moderate intersite U-U couplings. Also it is consistent with the study of the dilute  $U_x\text{Th}_{1-x}\text{Ru}_2\text{Si}_2$  alloys ( $0 \leq x \leq 0.07$ ) by Amitsuka and Sakakibara, which indicates that the lowest CEF state of  $5f$  electrons is magnetically degenerate due to the absence of saturation in the susceptibility of U contribution down to 100 mK.<sup>48</sup>

Choosing  $\Gamma_{t_5}^{(1)}$  as a lowest doublet, we explicitly write

$$|\uparrow\rangle = \cos\alpha|+3\rangle + \sin\alpha|-1\rangle, \quad (3.7)$$

$$|\downarrow\rangle = \cos\alpha|-3\rangle + \sin\alpha|+1\rangle, \quad (3.8)$$

with  $|M\rangle$  denoting the state of  $J_z = M$ . Operators  $J_z$ ,  $O_{x^2-y^2}$  and  $O_{xy}$  are represented within the subspace as

$$J_z = (3\cos^2\alpha - \sin^2\alpha) \begin{pmatrix} 1 & 0 \\ 0 & -1 \end{pmatrix}, \quad (3.9)$$

$$O_{x^2-y^2} = \sqrt{3}\sin\alpha(5\sin\alpha + 3\sqrt{7}\cos\alpha) \begin{pmatrix} 0 & 1 \\ 1 & 0 \end{pmatrix}, \quad (3.10)$$

$$O_{xy} = \sqrt{3}\sin\alpha(-5\sin\alpha + 3\sqrt{7}\cos\alpha) \begin{pmatrix} 0 & -i \\ i & 0 \end{pmatrix}. \quad (3.11)$$

The intersite interaction induces the AFQ ordering or the AFM ordering.

For the AFQ ordering, the ground state is given by an alternating array of the states  $|+\rangle$  and  $|-\rangle$ , where

$$|\pm\rangle = \sqrt{\frac{1}{2}}[|\uparrow\rangle \pm |\downarrow\rangle], \quad (3.12)$$

for the  $O_{x^2-y^2}$  ordering, and

$$|\pm\rangle = \sqrt{\frac{1}{2}}[|\uparrow\rangle \pm i|\downarrow\rangle], \quad (3.13)$$

for the  $O_{xy}$  ordering.

For the AFM ordering, the ground state is just an alternating array of  $|\uparrow\rangle$  and  $|\downarrow\rangle$ . The staggered magnetic moment is evaluated from

$$\mu/\mu_B = \cos^2\alpha|\langle+3|L_z+2S_z|+3\rangle| + \sin^2\alpha|\langle-1|L_z+2S_z|-1\rangle|. \quad (3.14)$$

Putting  $\alpha \simeq 52.48^\circ$  or  $\alpha \simeq 68.95^\circ$ , we obtain  $\mu \simeq 0.4\mu_B$ , close to the experimental value.<sup>24,25</sup>

### 3.2 The intermediate state

The  $E_1$  transition causes a  $3d$ -core electron to an unoccupied  $5f$  states, leading to the  $(3d)^9(5f)^3$ -configuration. The Slater integrals and the SOI parameters are evaluated within the HFA, which are also summarized in Table I.<sup>45</sup> The Coulomb interactions and the SOI of  $3d$  and  $5f$  electrons are represented within  $364 \times (2j_d + 1)$  states in the  $(3d)^9(5f)^3$ -configuration to construct the Hamil-

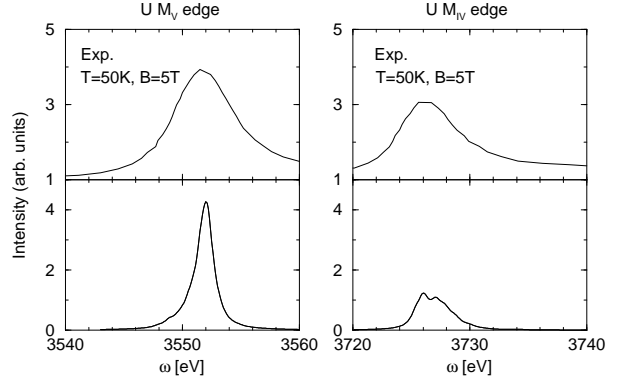


Fig. 3. Absorption coefficient as a function of the photon energy near U  $M_{1V}$  and U  $M_V$  edges. The upper panel is the experimental result (Ref. 48) and the lower panel is the calculated result.

tonian, and the intermediate state  $|\Lambda\rangle$  is calculated by diagonalizing the Hamiltonian. Here  $j_d = \frac{3}{2}$  and  $\frac{5}{2}$  mean the total moment of the  $3d$ -core electron from the  $M_{1V}$  and  $M_V$  edges, respectively. The CEF energy is so small in comparison with the multiplet energies that it can be neglected in the intermediate state. Then the energy levels are degenerate with respect to the magnetic quantum number  $M$  within the space of the total angular momentum  $J$ .

## 4. Calculated Results

### 4.1 Absorption coefficient

We discuss the absorption coefficient  $A(\omega)$  at U  $M_{1V}$  and  $M_V$  edges. Within the  $E_1$  transition, it is expressed as

$$A(\omega) \propto \sum_j \sum_{\Lambda} \sum_{\alpha} |\langle\Lambda|x_{\alpha}(j)|\psi_0\rangle|^2 \frac{\Gamma}{(\hbar\omega - E_{\Lambda})^2 + \Gamma^2}. \quad (4.15)$$

We calculate  $A(\omega)$  by assuming the AFQ ordering or the AFM ordering at zero temperature. The final state of photoabsorption is the same as the intermediate state of the RXS explained in the preceding section. The  $\Gamma$  is assumed to be 0.5 eV. Figure 3 shows the calculated result in comparison with the experiment.<sup>49</sup> The core-level energy is adjusted such that the calculated peak position coincides with that of the experimental peak position. The obtained spectra are independent of the choice of the ordered phase, which can be verified by means of the results obtained in Appendix. The broad peak is due to multiplet structure of the final state.

### 4.2 RXS Spectra

#### 4.2.1 AFQ phase

Assuming the AFQ phase in the initial state and using the intermediate state in the preceding section, we calculate the RXS spectra at U  $M_{1V}$  and  $M_V$  edges from eq. (2.2). The scattering amplitude has a form

$$M(\mathbf{G}, \omega) \propto \xi'(\omega) \begin{pmatrix} 1 & 0 & 0 \\ 0 & -1 & 0 \\ 0 & 0 & 0 \end{pmatrix}, \quad \text{for } O_{x^2-y^2} \text{ ordering}, \quad (4.16a)$$

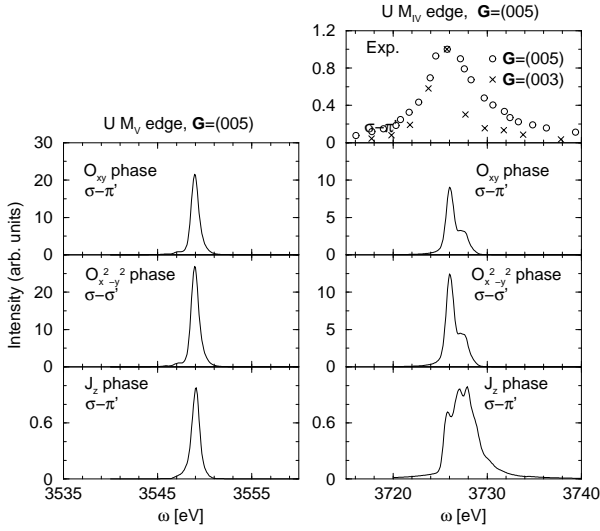


Fig. 4. The RXS spectra as a function of the photon energy at  $\mathbf{G} = (005)$  with  $\psi = 0$ . Left and right panels show the results around  $U M_V$  edge and  $M_{IV}$  edge, respectively. Top right panel shows the experimental result.<sup>41,50</sup> The rests are calculated results corresponding to those in the  $J_z$ ,  $O_{x^2-y^2}$  and  $O_{xy}$  phases from bottom to top, respectively, for both sides of the panels.

$$\propto \xi'(\omega) \begin{pmatrix} 0 & 1 & 0 \\ 1 & 0 & 0 \\ 0 & 0 & 0 \end{pmatrix}, \quad \text{for } O_{xy} \text{ ordering.} \quad (4.16b)$$

Combining these expressions with the geometrical factors in eq. (2.1), we obtain the intensities for  $\mathbf{G} = (00\ell)$

$$I_{\sigma \rightarrow \mu'} \propto \begin{cases} \cos^2(2\psi), & \mu' = \sigma' \\ \sin^2(2\psi) \sin^2 \theta, & \mu' = \pi' \end{cases}, \quad (4.17)$$

for the  $O_{x^2-y^2}$  ordering, and

$$I_{\sigma \rightarrow \mu'} \propto \begin{cases} \sin^2(2\psi), & \mu' = \sigma' \\ \cos^2(2\psi) \sin^2 \theta, & \mu' = \pi' \end{cases}, \quad (4.18)$$

for the  $O_{xy}$  ordering.

We find that the spectral shapes as a function of energy are independent of the assumed level schemes, although the intensities are quite different between the schemes.<sup>43</sup> Figure 4 shows the RXS spectra at  $\mathbf{G} = (005)$  with  $\psi = 0$  near  $U M_{IV}$  and  $M_V$  edges, as a function of photon energy. For the  $M_{IV}$  edge, the spectra have a width of  $\sim 5$  eV due to the multiplet structure in the intermediate state; a large peak is at  $\hbar\omega = 3.726$  keV. and a shoulder is at  $\sim 2$  eV higher than the peak. The calculated width looks somewhat narrower than the experimental one.<sup>41,50</sup> For the  $M_V$ , a narrower peak is found at  $\hbar\omega = 3.549$  keV.

As clear from eqs. (4.17) and (4.18), the RXS intensity depends considerably on the azimuthal angle. Figure 5 demonstrates this dependence. This is in contrast with the RXS intensity in the AFM state, where it shows no  $\psi$  dependence as shown below.

#### 4.2.2 AFM phase

We also calculate the RXS spectra, assuming the AFM phase in the initial state. The scattering amplitude

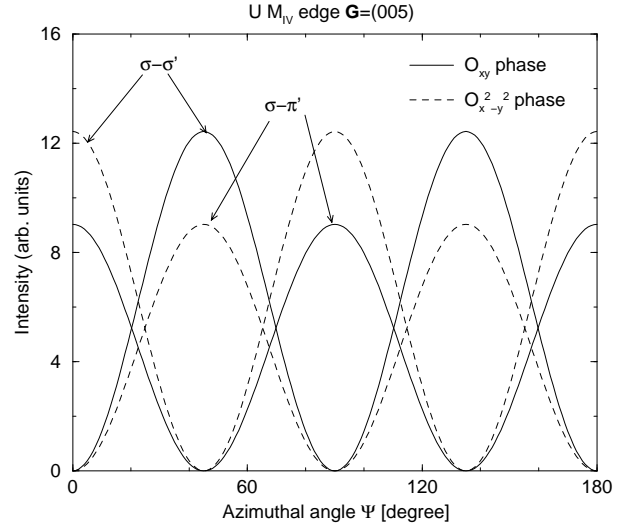


Fig. 5. Azimuthal angle dependence of the RXS peak intensities at  $\mathbf{G} = (005)$  near  $U M_{IV}$  edge in the AFQ phases. The solid and broken lines represent the results obtained in the  $O_{xy}$  and  $O_{x^2-y^2}$  orderings within the doublet scheme, respectively. The mixing angle is fixed to being  $\alpha \simeq 52.48^\circ$  and both  $\sigma - \sigma'$  and  $\sigma - \pi'$  channels are shown.

$M(\mathbf{G}, \omega)$  has a form

$$M(\mathbf{G}, \omega) \propto \begin{pmatrix} 0 & \xi(\omega) & 0 \\ -\xi(\omega) & 0 & 0 \\ 0 & 0 & 0 \end{pmatrix}. \quad (4.19)$$

Combining this with the geometrical factors in eq. (2.1), we can verify that the RXS intensities show no signal in the  $\sigma - \sigma'$  channel while those in the  $\sigma - \pi'$  channel remain constant with varying azimuthal angle  $\psi$ . This azimuthal angle dependence is valid as long as the scattering vector is in the form of  $(00\ell)$ .

As the same as the case of AFQ state, we find that the spectral shapes as a function of photon energy are independent of the assumed level schemes.<sup>43</sup> The RXS spectra at  $\mathbf{G} = (005)$  near  $U M_{IV}$  and  $M_V$  edges are shown in Fig. 4. The spectral peak is located at position  $\sim 2$  eV higher than that in the AFQ state, and the shoulder is seen at the lower energy side. This spectral shape is clearly different from that in the AFQ state. Unfortunately, the experimental spectra are not clear enough to distinguish the difference.

## 5. Concluding Remarks

We have analyzed the RXS spectra near  $U M_{IV}$  and  $M_V$  edges on the basis of a localized CEF model. By employing two level schemes, the singlet model of Santini and Amoretti and the doublet model of Ohkawa and Shimizu, we have considered the AFQ phase as a candidate of the HO phase and the AFM phase as the one realized under high pressure  $p > 1.5$  GPa. We have calculated the RXS spectra by taking into account the full Coulomb and spin-orbit interaction within the initial  $(3d)^{10}(5f)^2$  and intermediate  $(3d)^9(5f)^3$  configurations.

We have found that the spectral shapes as a function of photon energy are the same in both schemes. This looks unexpected, because the wave functions of the ini-

tial state are different between the schemes. Our numerical finding can be proved if the crystal field energy is negligible in the intermediate state, as given in Appendix.

The obtained spectra show strong differences between U  $M_{IV}$  and  $M_V$  edges, the former exhibits the broader and more complicated (multi-peak structure) profile than the latter as a function of photon energy. Also the spectral shapes are found quite different between the AFQ phase and the AFM phase. These differences as well as the photon polarization dependence may provide useful guidance to elucidate the symmetrical aspects of the actual system when the RXS experiment will be performed in high pressure phase.

The spectral shape calculated in the AFQ phase as a function of photon energy seems consistent with the experimental one at ambient pressure. On the other hand, the spectra have to depend on the azimuthal angle, as shown in Fig. 5. Quite recently, Bernhoeft *et al.* studied the azimuthal angle dependence of the peak intensity on the (005) magnetic spot in URu<sub>2</sub>Si<sub>2</sub>,<sup>50</sup> having claimed that the spectra show no azimuthal angle dependence. Mixture of phases of the  $O_{x^2-y^2}$  ordering and the  $O_{xy}$  ordering may make the spectra less depending on the azimuthal angle. Otherwise this may rule out the AFQ type ordering as a possible HO candidate.

Finally, URu<sub>2</sub>Si<sub>2</sub> is considered to be located at the borderline between a localized and an itinerant description. The CEF framework adopted in this work is to be seen only as a first approximation for the comprehensive understanding of the complex physics of this compound. The effort to this direction will be the next study.

## Acknowledgments

We would like to thank H. Amitsuka and M. Yokoyama for valuable discussions. J.I. thanks Max-Planck Institute for the Physics of Complex Systems for hospitality during his stay, where this work was completed. This work was partially supported by a Grant-in-Aid for Scientific Research from the Ministry of Education, Science, Sports and Culture.

## Appendix: Properties of the Scattering Amplitude

In this appendix, we derive general expressions of the matrix elements of the scattering amplitude in the  $E_1$  process, assuming that the intermediate state maintains rotational symmetry. This assumption seems reasonable when the CEF energy is negligible compared with the magnitude of the multiplet splitting in the intermediate state. Such conditions would be satisfied in many rare earth metal compounds. We show that the obtained expressions lead us to a useful limit on the shape of the RXS spectra as a function of the photon energy; it depends only on the type of the order parameter. We will not discuss the case of the  $E_2$  transition, since any useful limits on the spectral shape have not been derived from a similar discussion applied to this case. Although a similar discussion had been done by Lovesey and Balcar,<sup>51</sup> we treat rigorously the energy denominator appeared in the eq. (2.2), which is set aside in ref.51, in order to investigate the energy dependence of the RXS spectra.

### A.1 General results

First, we rewrite the scattering tensor in eq. (2.2) as

$$M_{\alpha\alpha'}(\mathbf{G}, \omega) = \frac{1}{\sqrt{N}} \sum_j e^{-i\mathbf{G}\cdot\mathbf{r}_j} \tilde{M}_{\alpha\alpha';j}(\omega), \quad (\text{A}\cdot 1)$$

$$\tilde{M}_{\alpha\alpha';j}(\omega) \equiv \sum_{\Lambda} E(\omega, \Lambda) \langle \psi_0 | x_{\alpha}(j) | \Lambda \rangle \langle \Lambda | x_{\alpha'}(j) | \psi_0 \rangle, \quad (\text{A}\cdot 2)$$

$$E(\omega, \Lambda) \equiv \frac{1}{\hbar\omega - (E_{\Lambda} - E_0) + i\Gamma}. \quad (\text{A}\cdot 3)$$

Note that contributions from the sites belonging to the same sublattice are the same. We omit the subscript  $j$  in the following. The initial state can be expanded by a linear combination of  $|J, m\rangle$  as

$$|\psi_0\rangle = \sum_m c(m) |J, m\rangle, \quad (\text{A}\cdot 4)$$

within a ground multiplet of  $J$  with  $m$  being the eigenvalue of  $J_z$ . If the rotational invariance is preserved in the intermediate state, the eigenstates  $|\Lambda\rangle$  are those of  $J^2$  and  $J_z$  simultaneously. (Of course the intermediate state is occupied by a core hole.) Notice that for a given value of  $J$ , there exist more than one multiplets having the same  $J$  value but having the different energy. Therefore we introduce variable  $i$  telling from the multiplets with the same value of  $J$ , and write the intermediate state as  $|\Lambda\rangle = |J', m', i\rangle$ . Then eq. (A.2) is written as

$$\tilde{M}_{\alpha\alpha'}(\omega) = \sum_{m, m'} c^*(m) c(m') \hat{M}_{\alpha\alpha'}^{m, m'}(\omega), \quad (\text{A}\cdot 5)$$

$$\begin{aligned} \hat{M}_{\alpha\alpha'}^{m, m'}(\omega) \equiv & \sum_{J'} \sum_{i=1}^{N_{J'}} \sum_{M=-J'}^{J'} E_i(\omega, J') \\ & \times \langle J, m | x_{\alpha} | J', M, i \rangle \langle J', M, i | x_{\alpha'} | J, m' \rangle, \end{aligned} \quad (\text{A}\cdot 6)$$

where  $E_i(\omega, J')$  represents  $E(\omega, \Lambda)$  in eq. (A.2). The number of the multiplets having the value  $J$  is denoted by  $N_J$ . The selection rule for the  $E_1$  process confines the range of the summation over  $J'$  to  $J' = J, J \pm 1$ . The evaluation of the matrix element of the type  $\langle J, m | x_{\alpha} | J', m' \rangle$  is yielded by utilizing the Wigner-Eckart theorem for a vector operator.<sup>52</sup> We write down several results derived from  $\hat{M}_{\alpha\alpha'}^{m, m'}(\omega)$  in the following.

First,  $\hat{M}_{\alpha\alpha'}^{m, m'}(\omega) \neq \mathbf{0}$  only when  $|m - m'| \leq 2$ . It is obvious because of the nature of the dipole operators. Second, for  $m' = m$ ,

$$\hat{M}^{m, m}(\omega) = \begin{pmatrix} a_m(\omega) & m\alpha(\omega) & 0 \\ -m\alpha(\omega) & a_m(\omega) & 0 \\ 0 & 0 & b_m(\omega) \end{pmatrix}, \quad (\text{A}\cdot 7)$$

$$\begin{aligned} a_m(\omega) = & [J(J+1) + m^2] F_{J-1}(\omega) \\ & + [J(J+1) - m^2] F_J(\omega) \\ & + [J(J+3) + m^2 + 2] F_{J+1}(\omega), \end{aligned} \quad (\text{A}\cdot 8)$$

$$\begin{aligned} b_m(\omega) = & (J^2 - m^2) F_{J-1}(\omega) + m^2 F_J(\omega) \\ & + [J(J+2) - m^2 + 1] F_{J+1}(\omega), \end{aligned} \quad (\text{A}\cdot 9)$$

$$\begin{aligned} \alpha(\omega) &= -(2J+1)F_{J-1}(\omega) \\ &\quad - F_J(\omega) + (2J+3)F_{J+1}(\omega), \end{aligned} \quad (\text{A}\cdot 10)$$

$$F_{J'}(\omega) \equiv |(J||V_1||J')|^2 \sum_{i=1}^{N_{J'}} E_i(\omega, J'), \quad (\text{A}\cdot 11)$$

where  $(J||V_1||J')$  denotes the reduced matrix element of the set of irreducible tensor operator of the first rank. Note that the diagonal elements satisfy the relations

$$a_m(\omega) = a_{-m}(\omega), \quad b_m(\omega) = b_{-m}(\omega). \quad (\text{A}\cdot 12)$$

One remarkable feature is that the off-diagonal elements are just proportional to  $m$ , completely factorized by the same function  $\alpha(\omega)$ . Another important result is that the trace is independent of  $m$

$$\begin{aligned} \text{Tr}[M^{m,m}(\omega)] &= 2a_m(\omega) + b_m(\omega) \\ &= J(2J+1)F_{J-1}(\omega) + J(J+1)F_J(\omega) \\ &\quad + [J(2J+5)+1]F_{J+1}(\omega), \end{aligned} \quad (\text{A}\cdot 13)$$

where  $\text{Tr}X$  is the trace of a quantity  $X$ .

Third, when  $|m' - m| = 2$ , we can derive the following results.

$$\hat{M}^{m,m+2} = a''_m \alpha''(\omega) \begin{pmatrix} 1 & i & 0 \\ i & -1 & 0 \\ 0 & 0 & 0 \end{pmatrix}, \quad (\text{A}\cdot 14)$$

$$\hat{M}^{m+2,m} = a''_m \alpha''(\omega) \begin{pmatrix} 1 & -i & 0 \\ -i & -1 & 0 \\ 0 & 0 & 0 \end{pmatrix}, \quad (\text{A}\cdot 15)$$

$$\begin{aligned} a''_m &= \sqrt{(J-m)(J+m+1)} \\ &\quad \times \sqrt{(J-m-1)(J+m+2)}, \end{aligned} \quad (\text{A}\cdot 16)$$

$$\alpha''(\omega) \equiv -F_{J-1}(\omega) + F_J(\omega) - F_{J+1}(\omega). \quad (\text{A}\cdot 17)$$

Here, we can see the energy dependence is factorized by the same function  $\alpha''(\omega)$  for every  $m$ . From these results, we can check  $a''_{-(m+2)} = a''_m$  holds, which leads us to the following relation

$$\hat{M}^{m,m\pm 2}(\omega) = \hat{M}^{-(m\pm 2),-m}(\omega), \quad (\text{A}\cdot 18)$$

where either all the upper or all the lower signs are to be taken.

Finally, for another  $m' \neq m$  case, that is, for  $|m' - m| = 1$ , the scattering amplitudes take forms

$$\hat{M}^{m,m+1}(\omega) = \begin{pmatrix} 0 & 0 & a'_m(\omega) \\ 0 & 0 & ia'_m(\omega) \\ b'_m(\omega) & ib'_m(\omega) & 0 \end{pmatrix}, \quad (\text{A}\cdot 19)$$

$$\hat{M}^{m+1,m}(\omega) = \begin{pmatrix} 0 & 0 & b'_m(\omega) \\ 0 & 0 & -ib'_m(\omega) \\ a'_m(\omega) & -ia'_m(\omega) & 0 \end{pmatrix}. \quad (\text{A}\cdot 20)$$

Actual forms of  $a'_m(\omega)$  and  $b'_m(\omega)$  can be obtained, but are not listed here because they are irrelevant to our present interest. We only notice that the matrix elements  $a'_m(\omega)$  and  $b'_m(\omega)$  cannot separate their arguments  $\omega$  and  $m$ .

## A.2 Application to $URu_2Si_2$

In the AFM phase, the relevant contributions to the RXS amplitude stem from the terms  $\hat{M}^{m,m}(\omega) - \hat{M}^{-m,-m}(\omega) \propto m\alpha(\omega)$ , which justifies the matrix form given by eq. (4.19). A detailed calculation reveals that the amplitude is proportional to the expectation value  $\langle J_z \rangle$ .

In the AFQ phases, on the other hand, the relevant contributions to the RXS amplitude come from the terms  $\hat{M}^{m,m+2}(\omega) \pm \hat{M}^{m+2,m}(\omega) \propto a''_m \alpha''(\omega)$  where a plus sign corresponds to the  $O_{x^2-y^2}$  phase while a minus sign corresponds to the  $O_{xy}$  phase. This also verifies the scattering amplitudes are given by eqs. (4.16a) and (4.16b). In these ordering phases, the energy dependence of the scattering amplitude is factorized by a single function  $\alpha(\omega)$  in the AFM phase or  $\alpha''(\omega)$  in the AFQ phase. This is the reason why the shape of the RXS spectra depends only on the type of the order parameter. Note that this factorization is special for the  $E_1$  transition in the present model. If terms  $\hat{M}^{m,m\pm 1}(\omega)$  become relevant for some physical reason, the factorization breaks down due to the presence of the elements  $a'_m(\omega)$  and  $b'_m(\omega)$ . We can see that the situation is more complicated for the  $E_2$  transition.

Since the true nature of the hidden order phase is unknown, it might be useful to consider what happens if some octupolar phase is substantiated in  $URu_2Si_2$ . Assuming two components of the octupolar ordering  $T_{xyz}$  and  $T_z^\beta$ , we can calculate the RXS signal from the octupole phase. For instance, we choose the initial states as these ordering phases in the singlet scheme and apply the results obtained in this appendix. The result says no RXS signal is detected in the antiferrooctupolar phase.

- 1) W. Schlabit, J. Baumann, B. Pollit, U. Rauchschwalbe, H. M. Mayer, U. Ahlheim and C. D. Bredl: *Z. Phys. B* **62** (1986) 171.
- 2) T. T. M. Palstra, A. A. Menovsky, J. v. d. Berg, A. J. Dirkmaat, P. H. Kes, G. J. Nieuwenhuys and J. A. Mydosh: *Phys. Rev. Lett.* **55** (1985) 2727.
- 3) Y. Miyako, S. Kawarazaki, H. Amitsuka, C. C. Paulsen and K. Hasselbach: *J. Appl. Phys.* **70** (1991) 5791.
- 4) A. P. Ramirez, P. Coleman, P. Chandra, E. Brck, A. A. Menovsky, Z. Fisk and E. Bucher: *Phys. Rev. Lett.* **68** (1992) 2680.
- 5) A. de Visser, F. E. Kay, A. A. Menovsky, J. J. M. Franse, J. van den Berg and G. J. Nieuwenhuys: *Phys. Rev. B* **34** (1986) 8168.
- 6) T. T. M. Palstra, A. A. Menovsky and J. A. Mydosh: *Phys. Rev. B* **33** (1986) 6527.
- 7) C. Broholm, J. K. Kjems, W. J. L. Buyers, P. Matthews, T. T. M. Palstra, A. A. Menovsky and J. A. Mydosh: *Phys. Rev. Lett.* **58** (1987) 1467.
- 8) D. E. MacLaughlin, D. W. Cooke, R. H. Heffner, R. L. Hutson, M. W. McElfresh, M. E. Schillaci, H. D. Rempp, J. L. Smith, J. O. Willis, E. Zirngiebl, C. Boekema, R. L. Lichti and J. Oostens: *Phys. Rev. B* **37** (1988) 3153.
- 9) B. Fåk, C. Vettier, J. Flouquet, F. Bourdarot, S. Raymond, A. Vernière, R. Lejay, Ph. Boutouille, N. R. Bernhoeft, S. T. Bramwell, R. A. Fischer and N. E. Phillips: *J. Magn. Magn. Mater.* **154** (1996) 339.
- 10) T. E. Mason and W. J. L. Buyers: *Phys. Rev. B* **43** (1991) 11471.
- 11) T. E. Mason, W. J. L. Buyers, T. Petersen, A. A. Menovsky and J. D. Garret: *J. Phys.: Condens. Matter* **7** (1995) 5089.
- 12) N. Shah, P. Chandra, P. Coleman and J. A. Mydosh: *Phys.*

- Rev. B **61** (2000) 564.
- 13) P. Santini and G. Amoretti: Phys. Rev. Lett. **73** (1994) 1027.
  - 14) P. Santini: Phys. Rev. B **57** (1998) 5191.
  - 15) A. Tsuruta, A. Kobayahi, T. Matsuura and Y. Kuroda: J. Phys. Soc. Jpn. **69** (2000) 663.
  - 16) Y. Takahashi: J. Phys. Soc. Jpn. **70** (2001) 2226.
  - 17) F. J. Ohkawa and H. Shimizu: J. Phys.: Condens. Matter **11** (1999) L519.
  - 18) V. Barzykin and L. P. Gor'kov: Phys. Rev. Lett. **74** (1995) 4301.
  - 19) H. Ikeda and Y. Ohashi: Phys. Rev. Lett. **81** (1998) 3723.
  - 20) P. Chandra, P. Coleman and J. A. Mydosh: Physica B **312-313** (2002) 397.
  - 21) P. Chandra, P. Coleman and J. A. Mydosh and V. Tripathi: Nature **417** (2002) 831.
  - 22) P. Chandra, P. Coleman and J. A. Mydosh and V. Tripathi: J. Phys.: Condens. Matter **15** (2003) S1965.
  - 23) T. Kasuya: J. Phys. Soc. Jpn. **66** (1997) 3348.
  - 24) H. Amitsuka, M. Sato, N. Metoki, M. Yokoyama, K. Kuwahara, T. Sakakibara, H. Moritomo, S. Kawarazaki, Y. Miyako and J. A. Mydosh: Phys. Rev. Lett. **83** (1999) 5114.
  - 25) H. Amitsuka, M. Yokoyama, K. Tenya, T. Sakakibara, K. Kuwahara, M. Sato, N. Metoki, T. Honma, Y. Ōnuki, S. Kawarazaki, Y. Miyako, S. Ramakrishnan and J. A. Mydosh: J. Phys. Soc. Jpn. Suppl. **69** (2000) 5.
  - 26) K. Matsuda, Y. Kohori, T. Kohara, K. Kuwahara and H. Amitsuka: Phys. Rev. Lett. **87** (2001) 087203.
  - 27) K. Matsuda, Y. Kohori, T. Kohara, H. Amitsuka, K. Kuwahara and T. Matsumoto: J. Phys.: Condens. Matter **15** (2003) 2363.
  - 28) G. Motoyama, T. Nishioka and N. K. Kato: Phys. Rev. Lett. **90** (2003) 166402.
  - 29) M. Yokoyama, H. Amitsuka, K. Watanabe, S. Kawarazaki, H. Yoshizawa and J. A. Mydosh: J. Phys. Soc. Jpn. Suppl. **71** (2002) 264.
  - 30) H. Nakao, K. Magishi, Y. Wakabayashi, Y. Murakami, K. Koyama, K. Hirota, Y. Endoh and S. Kunii: J. Phys. Soc. Jpn. **70** (2001) 1857.
  - 31) T. Nagao and J. Igarashi: J. Phys. Soc. Jpn. **70** (2001) 2892.
  - 32) J. Igarashi and T. Nagao: J. Phys. Soc. Jpn. **71** (2002) 1771.
  - 33) S. W. Lovesey: J. Phys.: Condens. Matter **14** (2002) 4415.
  - 34) Y. Tanaka, T. Inami, T. Nakamura, H. Yamauchi, H. Onodera, K. Ohyama and Y. Yamaguchi: J. Phys.: Condens. Matter **11** (1999) L505.
  - 35) K. Hirota, N. Oumi, T. Matsumura, H. Nakao, Y. Wakabayashi, Y. Murakami and Y. Endoh: Phys. Rev. Lett. **84** (2000) 2706.
  - 36) T. Matsumura, N. Oumi, K. Hirota, H. Nakao, Y. Murakami, Y. Wakabayashi, T. Arima, S. Ishihara and Y. Endoh: Phys. Rev. B **65** (2002) 094420.
  - 37) J. Igarashi and T. Nagao: J. Phys. Soc. Jpn. **72** (2003) 1279.
  - 38) I. S. Elfimov, V. I. Anisimov and G. Sawatzky: Phys. Rev. Lett. **82** (1999) 4264.
  - 39) M. Benfatto, Y. Joly and C. R. Natoli: Phys. Rev. Lett. **83** (1999) 636.
  - 40) M. Takahashi, J. Igarashi and P. Fulde: J. Phys. Soc. Jpn. **68** (1999) 2530.
  - 41) E. D. Isaacs, D. B. McWhan, R. N. Kleiman, D. J. Bishop, G. E. Ice, P. Zschack, B. D. Gaulin, T. E. Mason, J. D. Garrett and W. J. L. Buyers: Phys. Rev. Lett. **65** (1990) 3185.
  - 42) E. Lidström, D. Mannix, A. Hiess, J. Rebizant, F. Wastin, G. H. Lander, I. Marri, P. Carra, C. Vettier and M. J. Longfield: Phys. Rev. B **61** (2000) 1375.
  - 43) This unexpected property can be proved if the intermediate state has rotational symmetry. This condition is satisfied within a good approximation if the crystal field energy is much smaller than the multiplet energy.
  - 44) T. Shishidou, T. Jo and T. Oguchi : unpublished.
  - 45) R. Cowan: *The Theory of Atomic Structure and Spectra* (University of California Press, Berkeley, 1981).
  - 46) T. E. Mason, B. D. Gaulin, J. D. Garrett, Z. Tun, J. L. Buyers and E. D. Isaacs: Phys. Rev. Lett. **65** (1990) 3189.
  - 47) The definitions of the components of the quadrupolar operators adopted in ref. 13 are different from those of the present work by a factor  $\sqrt{3}/2$ . Therefore, the value of the coupling constant  $\lambda$  in ref. 13 corresponds to  $4\lambda/3$  here.
  - 48) H. Amitsuka and T. Sakakibara: J. Phys. Soc. Jpn. **63** (1994) 736.
  - 49) A. Yaouanc, P. Dalmas de Réotier, G. van der Laan , A. Hiess, J. Goulon, C. Neumann and N. Sato: Phys. Rev. B **58** (1998) 8793.
  - 50) N. Bernhoeft, G. H. Lander, M. J. Longfield, S. Langridge, D. Mannix, E. Lidström, E. Colineau, A. Hiess, C. Vettier, F. Wastin, J. Rebizant and P. Lejay: Acta Physica Pol. B **34** (2003) 1367.
  - 51) S. W. Lovesey and E. Balcar: J. Phys.: Condens Matter **8** (1996) 10983.
  - 52) E. U. Condon and G. H. Shortley: *The Theory of Atomic Spectra* (Cambridge University Press, Cambridge, 1935).